

Nonlinear electrophoresis of colloids controlled by anisotropy of conductivity and permittivity of liquid crystal electrolyte

Sathyanarayana Paladugu¹, Christopher Conklin², Jorge Viñals², and Oleg D. Lavrentovich^{1†}

¹Liquid Crystal Institute and Chemical Physics Interdisciplinary Program,
Kent State University, Kent, OH 44242

²School of Physics and Astronomy,
University of Minnesota, Minneapolis, MN 55455

Abstract

Liquid crystal electrolytes enable nonlinear electrophoresis of colloidal particles with velocities proportional to the square of the applied field. We demonstrate that the magnitude and even the polarity of electrophoretic mobility can be controlled by the anisotropy of electric conductivity and dielectric permittivity of the liquid crystal. In particular, reversal of electrophoretic mobility can be triggered either by temperature or composition changes that alter the signs of the conductivity and permittivity anisotropies. Controllable reversal of mobility adds to the list of advantages of anisotropic electrolytes over their isotropic counterparts.

[†] olavrent@kent.edu

Microscale manipulation of colloidal particles and fluids by electric fields is a broad area of active scientific research ranging from fundamental studies of non-equilibrium phenomena [1-4] to the development of practical devices for informational displays, portable diagnostics, sensing, delivery, and sorting [5-7]. It has been demonstrated recently [4,8-10] that when a nematic liquid crystal is used as an electrolyte instead of an isotropic fluid, electrokinetic phenomena acquire qualitatively new characteristics. An important feature of the nematic electrolyte is that the space charge is generated in the medium, at the distortions of molecular orientations, rather than at the interface between the particle and the electrolyte. Space charge separation occurs in the applied electric field, which drives positive and negative ions to different regions of the deformed liquid crystal thanks to the anisotropy of conductivity and dielectric permittivity [8-10]. The electric field then imposes a Coulomb force on the charged clouds, setting the nematic into electrokinetic flows with the velocities growing as the square of the applied field E (one degree of E separates the charges, the other drives the flows) [8-10]. The quadratic dependence brings an important advantage of the liquid crystal-enabled electrokinetics (LCEK) over its isotropic linear counterpart since one can use an alternating current (AC) electric field as a driving force [9,11]. Furthermore, orientational order of the electrolyte allows one to design trajectories of the colloids by patterning the director \hat{n} that specifies local orientation of the liquid crystal [8,11].

Theoretically, the electrokinetic velocities are expected to depend on the anisotropy $\tilde{\epsilon} = \epsilon_{\parallel} / \epsilon_{\perp} - 1$ of permittivity and $\tilde{\sigma} = \sigma_{\parallel} / \sigma_{\perp} - 1$ of conductivity; the subscripts \parallel and \perp refer to the orientation parallel and perpendicular to \hat{n} , respectively [8-10]. For a sphere of

a radius R with perpendicular surface alignment of \hat{n} , the electrophoretic velocity is predicted to be [9]

$$v = \alpha \varepsilon_0 \varepsilon_{\perp} \eta_{\parallel}^{-1} (\tilde{\varepsilon} - \tilde{\sigma}) RE^2, \quad (1)$$

where ε_0 is permittivity in vacuum, η_{\parallel} is the effective nematic viscosity, and α is a numerical parameter of the order of 1 that should depend on the details of director configuration, finite surface anchoring, anisotropy of viscoelastic parameters of the nematic; its exact theoretical value is not known. Although the experiments support the model in the part of $v \propto RE^2$ dependence [8,9,11-14] and in the guiding effect of the director field [8,11,15-18], there are no experimental data on how v depends on $\tilde{\varepsilon}$ and $\tilde{\sigma}$, the two crucial properties of the nematic electrolyte. As predicted by Eq.(1), one can reverse the polarity of v by altering the sign of $(\tilde{\varepsilon} - \tilde{\sigma})$. Flow reversals have been observed in isotropic electrolytes but their mechanisms are not fully understood [1]. In the present work, we design experiments to verify the key element of LCEK mechanism, by using nematics with broadly varying $\tilde{\varepsilon}$ and values of $(\tilde{\varepsilon} - \tilde{\sigma})$ that reverse their sign as a function of temperature. We demonstrate that $v \propto (\tilde{\varepsilon} - \tilde{\sigma})$, as predicted by Eq.(1), and can reverse its sign as a function of composition and temperature.

Materials. We used binary mixtures of room-temperature nematics pentylcyanobiphenyl (5CB) and HNG715600-100 (purchased from Jiangsu Hecheng Display Technology and referred to as HNG in what follows). 5CB exhibits $\tilde{\varepsilon} = 1.9$ [19] and HNG exhibits $\tilde{\varepsilon} = -0.7$ [20] at room temperature. Concentration variation of mixtures

changes ($\tilde{\varepsilon} - \tilde{\sigma}$) strongly, both in absolute value and in sign. Dry soda-lime-silica spheres of diameter $2R = (9.6 \pm 1) \mu\text{m}$ (purchased from ThermoScientific) were used as electrophoretic particles. The spheres were treated with dimethyloctadecyl[3-(trimethoxysilyl)propyl]ammonium chloride (DMOAP) to impart perpendicular orientation of $\hat{\mathbf{n}}$. The nematic layers of thickness $h = 60 \mu\text{m}$ were confined between two glass plates with planar alignment, $\hat{\mathbf{n}}_0 = (1, 0, 0)$, achieved by rubbed polymer coating (PI-2555, purchased from HD Microsystems). The temperature was controlled by Linkam controller TMS94 and a hot stage LTS350 (Linkam Scientific Instruments) with accuracy $\pm 0.01^\circ\text{C}$.

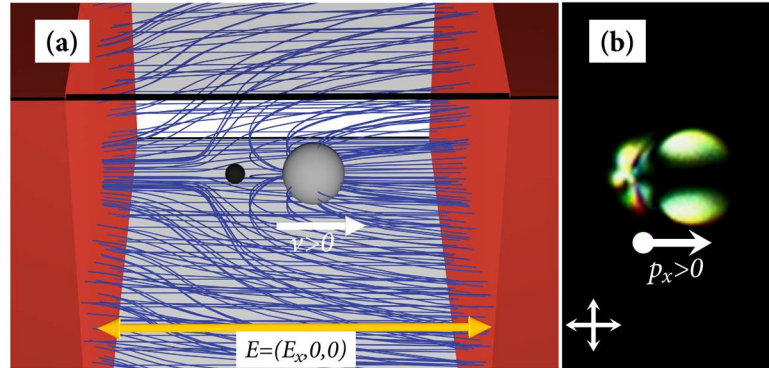


Figure 1. (a) Scheme of electrophoresis for the case $(\tilde{\varepsilon} - \tilde{\sigma}) > 0$; (b) microphotograph of a glass sphere with a point defect “hedgehog” (located on the left) placed in the nematic LC, seen between cross polarizers. The structural dipole $\vec{p} = (p_x, 0, 0)$ is shown by arrow.

A sphere with perpendicular surface anchoring, placed in an uniform nematic, with the director along the x -axis, $\hat{\mathbf{n}}_0 = (1, 0, 0)$, produces a dipolar director field with a point defect, the so-called hyperbolic hedgehog [21], Figure 1. The hedgehog can form either on the left or right side of the sphere; once formed, it does not change sides since the energy

barrier is orders of magnitude higher than the thermal energy. We direct the structural dipole $\bar{\mathbf{p}}$ from the hedgehog towards the sphere, Figure 1b. The AC electric field of frequency 25 Hz was applied parallel to $\hat{\mathbf{n}}_0$ using two aluminum strips separated by a distance $L = 4 \text{ mm}$, Figure 1. The amplitude of the field acting on the particles in the center of the cells is $E = 19.75 \text{ mV} / \mu\text{m}$ which is 79% of the applied field (the reduction is caused by the difference of dielectric permittivities of glass plates and the nematic [9] and was determined by numerical simulations as described in Supplemental material).

Reversal of electrophoretic velocity v by composition. We designed the experiments in such a way that $\tilde{\epsilon}$ varied broadly from mixture to mixture while the anisotropy of conductivity remained constant, $\tilde{\sigma} = 0.4$. To achieve these conditions, the experiments were performed at the temperature $t = T - T_{NI} = -5^\circ\text{C}$ for each mixture, where T_{NI} is the temperature of the isotropic-nematic transition of that mixture, Figure 2a. At high weight concentrations of 5CB, $c > 0.54$, the spheres move with the sphere leading the way, $v > 0$, Figure 2b. For $c < 0.54$, the polarity is reversed, $v < 0$, i.e., the sphere follows the hedgehog, Figure 2b.

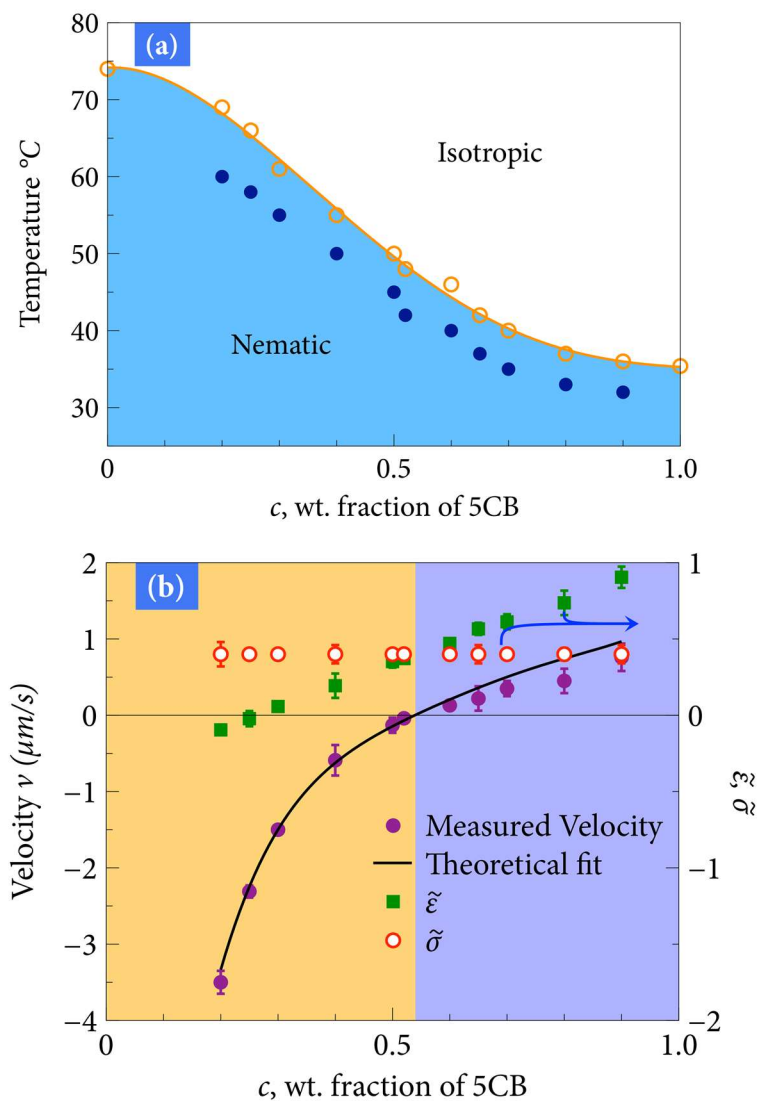


Figure 2. (a) Phase diagram of 5CB-HNG mixtures. Open circles show T_{NI} and the filled circles show the temperatures $t = T - T_{NI} = -5^\circ\text{C}$ at which the material parameters and electrophoretic velocities were measured; (b) Concentration dependence of electrophoretic velocity v , dielectric $\tilde{\epsilon}$ and conductivity $\tilde{\sigma}$ anisotropies; solid line is the fit of $v(c)$ by Eq. (1) with $\alpha = 1.1 \pm 0.2$.

Reversal of electrophoretic velocity v by temperature change. Analysis of the data in Figure 2 suggests that the polarity of electrophoresis can be reversed by simply changing the temperature of the nematic mixture with concentrations close to $c = 0.52$. Figure 3 shows that this is indeed the case, as the electrophoretic velocity changes from negative to positive as the temperature decreased, with $t_v \approx -7^\circ\text{C}$ being the point of reversal.

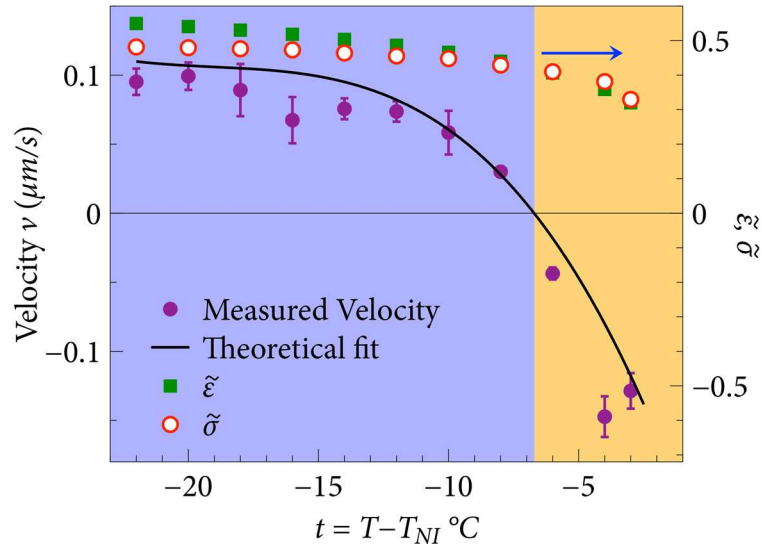


Figure 3. Temperature-triggered reversal of electrophoretic velocity v , plotted together with the temperature dependencies of $\tilde{\epsilon}$, and $\tilde{\sigma}$ for a binary mixture $c = 0.52$; the solid line is the fit of $v(t)$ by Eq.(1), with $\alpha = 1.2 \pm 0.2$.

To understand the physical reason of the velocity reversal, we performed a thorough characterization of the material properties entering Eq.(1), as described below.

Anisotropy of electric conductivity. The conductivity of nematics is of an ionic type [22,23]. To determine $\sigma_{\parallel} / \sigma_{\perp}$, we tracked transient currents in cells of thickness $15 \mu\text{m}$ with homeotropic and planar alignment, in response to a square wave voltage of frequency 1 Hz and amplitude $(4-7) \text{ V}$ [24]. The ratio of times required by the ions to migrate through the cell determines the ratio of ionic mobilities, which in its turn, yields $\sigma_{\parallel} / \sigma_{\perp}$ and thus $\tilde{\sigma}$. We find $\tilde{\sigma} \approx 0.4$ for all mixtures at $t = -5^{\circ}\text{C}$, Figure 2b.

Dielectric anisotropy. Static permittivities ε_{\parallel} and ε_{\perp} are measured using Solatron 1260 analyzer, at $t = -5^{\circ}\text{C}$, Figure 4a. These data are used to plot the function $\tilde{\varepsilon}(c)$ in Figure 2b that crosses $\tilde{\sigma}(c)$ at $c = 0.54$. For the mixture with $c = 0.52$, the dielectric permittivities are measured over the entire range of the nematic phase, Figure 5a; these data are used to construct the monotonous dependency $\tilde{\varepsilon}(t)$ in Figure 3.

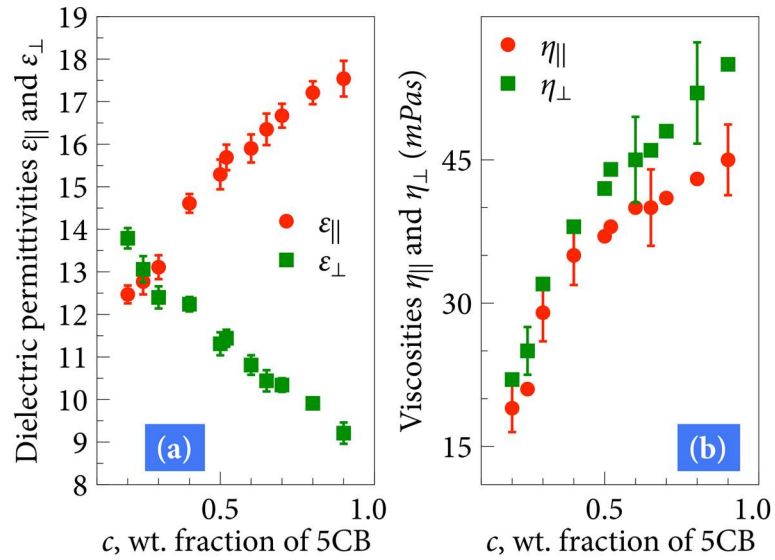


Figure 4. Concentration dependencies of dielectric permittivities and viscosity coefficients measured at $t = -5^{\circ}\text{C}$.

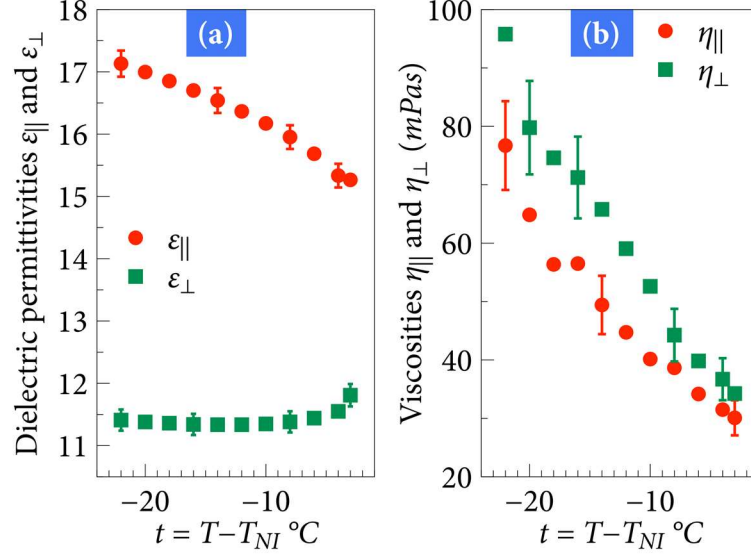


Figure 5. Temperature dependence of dielectric permittivities and viscosities of binary mixture at $c = 0.52$.

Viscosities. The effective viscosities $\eta_{||}$ and η_{\perp} , Figs.4b and 5b, for the displacements parallel and perpendicular to \hat{n}_0 , respectively, [25,26] are defined from the generalized Stokes-Einstein equation $\eta_{||,\perp} = k_B T / (6\pi R D_{||,\perp})$ by tracking Brownian trajectories of the same spheres as those in the electrophoretic experiments. Here k_B is the Boltzmann constant, T is the absolute temperature, $D_{||}$ and D_{\perp} are the two diffusion coefficients, measured from the time dependencies of the mean square displacements, $\langle \Delta x^2(\tau) \rangle = 2D_{||}\tau$ and $\langle \Delta y^2(\tau) \rangle = 2D_{\perp}\tau$, respectively. The time lag τ was longer than 100 ms to avoid anomalous regimes [27]. Both $\eta_{||}$ and η_{\perp} increase with c , Figure 4b. For the mixture with $c = 0.52$, both $\eta_{||}$ and η_{\perp} increase as the temperature is lowered, Figure 5b.

Correlation of velocity reversals and material properties: experimental data.

Comparative analysis of the dependencies $\tilde{\varepsilon}(c)$, $\tilde{\varepsilon}(t)$, $\tilde{\sigma}(c)$, $\tilde{\sigma}(t)$, $v(c)$ and $v(t)$ demonstrate a strong correlation between v and the material parameter $(\tilde{\varepsilon} - \tilde{\sigma})$, as predicted by Eq.(1). Namely, v is negative when $(\tilde{\varepsilon} - \tilde{\sigma})$ is negative and positive otherwise, Figure 2b and Figure 3. Moreover, the experimentally determined η_{\parallel} , ε_{\perp} , $\tilde{\varepsilon}$, $\tilde{\sigma}$, allowed us to fit both $v(c)$ and $v(t)$ dependencies with Eq.(1) very well, with the fitting parameter being the same within the experimental error, $\alpha = 1.1 \pm 0.2$ in Figure 2b and $\alpha = 1.2 \pm 0.2$ in Figure 3.

Equation (1) has been deduced in Ref.[9] without an explicit consideration of the exact director configuration caused by the surface anchoring at the surface of the spheres and director deformations that might be caused by the applied field through dielectric, surface polarization and flexoelectric mechanisms [28] and by viscous flow effects [29]. Below we discuss the relative importance of these distortions.

The field-induced realigning torques that deviate the director from the sphere-imposed direction by a small angle $\delta\theta$ can be estimated as $(K/\xi)\delta\theta$ for dielectric realignment and as $e^*E\delta\theta$ for the flexoelectric-surface polarization effect [28]; here K is the average Frank constant, $\xi = \sqrt{4\pi K / \Delta\varepsilon} / |E|$ is the dielectric extrapolation length, $e^* = e_1 + e_3 \pm P$ where e_1 and e_3 are the flexoelectric coefficients, P is the surface polarization; e^* can be as high as [28] $e^* \sim 10^{-10} \text{ C/m}$. For the cited electric fields, $K/\xi \sim 3 \times 10^{-8} \text{ J/m}^2$ and $e^*E \sim 2 \times 10^{-6} \text{ J/m}^2$. The latter value is not negligibly small

when compared to the expected polar anchoring strength ($10^{-6} - 10^{-4}$) J/m^2 [30-32] that is responsible to the appearance of the hedgehog next to the sphere of a diameter $2R \approx 10 \mu m$. The Ericksen number in the problem, estimated roughly as $Er = 2\eta Rv / K$, and characterizing a ratio of the viscous to the elastic stress, is of the order of 0.1 (for $\eta = 25 \text{ mPas}$ as, $v = 2 \mu m/s$). Thus both the field [28] and flow [29] might modify the director and influence α in Eq.(1). Another potential factor influencing α is the difference in dielectric permittivities of the colloid and the nematic, as it leads to gradients of the local electric field.

Correlation of velocity reversals and material properties: numerical simulations. In order to examine the correlation between the velocity and material properties, to gain further insight into the charge distribution and flow field induced by the applied field, and to test the effect of surface anchoring on director deformation, we have developed a computational model of the transport equations [33]. We consider a 2D geometry and neglect surface polarization and flexoelectric effects. Given the small Ericksen number, we use as input the variation solution for the nematic field around a sphere with homeotropic anchoring [21]. We then solve for the charge distribution and velocity fields under a uniform and oscillatory AC electric field. The particle is considered as immobilized, with a fixed location.

Figure 6 shows the instantaneous charge distribution when $\tilde{\epsilon} - \tilde{\sigma}$ is negative (Fig.6a) and positive (Fig.6b), and the corresponding flow fields (averaged over a period of the field), in Fig.6c and 6d, respectively. Despite differences in the details, the resulting

average flow fields for negative and positive $\tilde{\epsilon} - \tilde{\sigma}$ are very similar, except that the flows are completely reversed, as clear from the comparison of Fig. 6c and 6d in which the arrows indicate the velocity fields.

The left-right asymmetry of the director configuration around the colloid in Fig.6 leads to the pumping effect [8,9] along the x-axis parallel to the structural dipole $\vec{p} = (p_x, 0, 0)$. Under the action of the electric field, the nematic is pumped from one side of the colloid to another; there is no pumping in the orthogonal y-direction, Fig.6e and Fig.6f. When $\tilde{\epsilon} - \tilde{\sigma} < 0$, the nematic fluid around the immobilized sphere is pumped along the positive direction of the x-axis, Fig.6e, i.e. along \vec{p} . This polarity of the electroosmotic pumping should be opposite to the direction of the electrophoretic propulsion of a free sphere. In the experiment, the free particles in the medium with $\tilde{\epsilon} - \tilde{\sigma} < 0$ are indeed moving towards the negative direction of the x-axis, $v < 0$, with the hedgehog leading the way, Figs. 1, 2b, and 3. For the case $\tilde{\epsilon} - \tilde{\sigma} > 0$, polarities of electroosmotic pumping, Fig.6f, and of electrophoretic motion, Fig.2b,3, are reversed, as they should be. Therefore, the numerical simulations confirm the experimentally determined polarity of the electrophoretic motion.

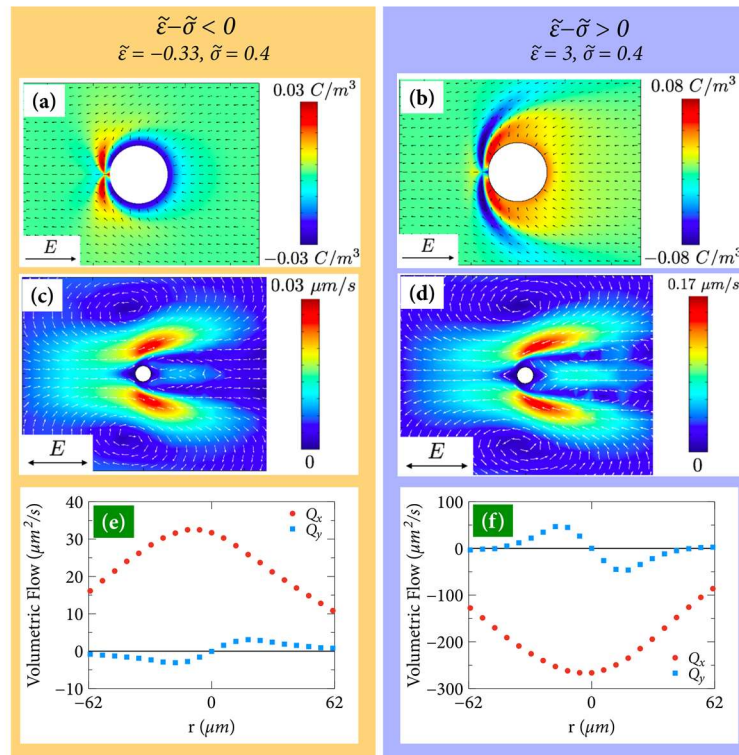


Figure 6 . Numerical solutions for LCEK flows around fixed particle in two dimensions for various dielectric anisotropies, with applied field parallel to the dipole. (a)-(b) Charge density plotted in color, with arrows representing the director field. (c)-(d) Corresponding flow velocity map, showing flow reversal as $\tilde{\epsilon} - \tilde{\sigma}$ changes sign (e)-(f) Volumetric flows along the x-axis (Q_x) and along the y-axis (Q_y) pumped around the particle by the electric field.

To summarize, the measured LCEK velocities show a linear dependence on the material parameters of the nematic electrolyte, namely, the dielectric and conductivity anisotropies, as expected from the theory, Eq.(1). The experiments demonstrate that each of these two anisotropies can cause LCEK. Anisotropy of conductivity guides the ions

along the pathways defined by the director, thus separating the charges in space. Dielectric anisotropy of a spatially distorted nematic acted upon by the electric field yields spatially varying local electric field; ions move in response to the nonuniform field pattern, thus creating the spatial charge. In both cases, the separated charges, acted upon by the field that created them, result in LCEK flows. Experimentally determined electrophoretic behavior of the free spheres and numerical simulations of the immobilized spheres show a good agreement with each other. In particular, the polarities of the electrophoretic velocities of free particles are opposite to those of the electro-osmotic flows around immobilized particles.

The nematic electrolytes allow one to control both the magnitude and the polarity of electrokinetic flows by simply tuning the temperature or composition to change the value of $\tilde{\epsilon} - \tilde{\sigma}$. We determined the numerical coefficient in Eq.(1) that connect the electrophoretic velocity to the material parameters, as $\alpha = 1.1 - 1.2$. Analysis of the experimental data also suggests that the next level of detailed description of LCEK in which α is derived as a function of surface anchoring strength, flexoelectric and surface polarization effects, etc., should account for the dynamic nature of the director deformations in the applied electric field and their modification by the flows.

Acknowledgements. We acknowledge fruitful discussions with M. C. Calderer, D. Golovaty, I. Lazo-Martinez, S. Shiyanovskii, O. M. Tovkach, and N. J. Walkington. We thank J. Xiang for the help in numerical simulations. The work was supported by NSF grant DMR-1410378 and the Minnesota Supercomputing Institute.

References.

- [1] M. Z. Bazant, M. S. Kilic, B. D. Storey, and A. Ajdari, *Advances in Colloid and Interface Science* **152**, 48 (2009).
- [2] I. S. Aranson, *Physics-Usppekhi* **56**, 79 (2013).
- [3] A. Zöttl and H. Stark, *Journal of Physics: Condensed Matter* **28**, 253001 (2016).
- [4] O. D. Lavrentovich, *Current Opinion in Colloid & Interface Science* **21**, 97 (2016).
- [5] J. Dobnikar, A. Snezhko, and A. Yethiraj, *Soft Matter* **9**, 3693 (2013).
- [6] A. Ramos, *Electrokinetics and Electrohydrodynamics in Microsystems* Springer-Verlag Wien, 2011), CISM International Centre for Mechanical Sciences, 530.
- [7] M. Z. Bazant and T. M. Squires, *Current Opinion in Colloid & Interface Science* **15**, 203 (2010).
- [8] C. Peng, Y. Guo, C. Conklin, J. Viñals, S. V. Shiyankovskii, Q.-H. Wei, and O. D. Lavrentovich, *Physical Review E* **92**, 052502 (2015).
- [9] I. Lazo, C. Peng, J. Xiang, S. V. Shiyankovskii, and O. D. Lavrentovich, *Nat Commun* **5** (2014).
- [10] O. M. Tovkach, M. C. Calderer, D. Golovaty, O. Lavrentovich, and N. J. Walkington, *Physical Review E* **94**, 012702 (2016).
- [11] O. D. Lavrentovich, I. Lazo, and O. P. Pishnyak, *Nature* **467**, 947 (2010).
- [12] S. Hernández-Navarro, P. Tierno, J. Ignés-Mullol, and F. Sagués, *Soft Matter* **9**, 7999 (2013).
- [13] S. Hernández-Navarro, P. Tierno, J. Ignés-Mullol, and F. Sagués, *The European Physical Journal Special Topics* **224**, 1263 (2015).
- [14] Y. Nishioka, F. Kobayashi, N. Sakurai, Y. Sasaki, and H. Orihara, *Liquid Crystals* **43**, 427 (2016).
- [15] I. Lazo and O. D. Lavrentovich, *Philosophical Transactions of the Royal Society of London A: Mathematical, Physical and Engineering Sciences* **371** (2013).
- [16] Y. Sasaki, H. Hoshikawa, T. Seto, F. Kobayashi, V. S. R. Jampani, S. Herminghaus, C. Bahr, and H. Orihara, *Langmuir* **31**, 3815 (2015).
- [17] S. Hernández-Navarro, P. Tierno, J. A. Farrera, J. Ignés-Mullol, and F. Sagués, *Angewandte Chemie International Edition* **53**, 10696 (2014).
- [18] Y. Sasaki, Y. Takikawa, V. S. R. Jampani, H. Hoshikawa, T. Seto, C. Bahr, S. Herminghaus, Y. Hidaka, and H. Orihara, *Soft Matter* **10**, 8813 (2014).
- [19] J. Jazdyn and P. Kêdziora, *Molecular Crystals and Liquid Crystals* **145**, 17 (1987).
- [20] B.-X. Li, V. Borshch, S. V. Shiyankovskii, S.-B. Liu, and O. D. Lavrentovich, *Applied Physics Letters* **104**, 201105 (2014).
- [21] P. Poulin, H. Stark, T. C. Lubensky, and D. A. Weitz, *Science* **275**, 1770 (1997).
- [22] G. Vertogen and W. H. de Jeu, *Thermotropic Liquid Crystals, Fundamentals* (Springer-Verlag Berlin, 1988).
- [23] K. Neyts and F. Beunis, in *Handbook of Liquid Crystals*, edited by J. W. Goodby *et al.* (Wiley-VCH Verlag GmbH & Co. KGaA, 2014), pp. 357.
- [24] G. H. Heilmeyer and P. M. Heyman, *Physical Review Letters* **18**, 583 (1967).
- [25] J. C. Loudet, P. Hanusse, and P. Poulin, *Science* **306**, 1525 (2004).
- [26] B. Senyuk, D. Glugla, and I. I. Smalyukh, *Physical Review E* **88**, 062507 (2013).
- [27] T. Turiv, I. Lazo, A. Brodin, B. I. Lev, V. Reiffenrath, V. G. Nazarenko, and O. D. Lavrentovich, *Science* **342**, 1351 (2013).

- [28] O. D. Lavrentovich, V. G. Nazarenko, V. V. Sergan, and G. Durand, *Physical Review A* **45**, R6969 (1992).
- [29] J.-I. Fukuda, H. Stark, M. Yoneya, and H. Yokoyama, *Journal of Physics: Condensed Matter* **16**, S1957 (2004).
- [30] Y. A. Nastishin, R. D. Polak, S. V. Shiyanovskii, V. H. Bodnar, and O. D. Lavrentovich, *Journal of Applied Physics* **86**, 4199 (1999).
- [31] L. M. Blinov, *Structure and Properties of Liquid Crystals* (Springer Netherlands, 2011).
- [32] T. Rasing and I. Muševič, *Surfaces and Interfaces of Liquid Crystals* (Springer Berlin Heidelberg, 2004).